Effects of Combined Additions of Mn and Zr on Dispersoid Formation and Recrystallization Behavior in Al-Zn-Mg Alloys

SHENGDAN LIU, JINGCHAO CHEN, WENRU CHAI, QING WANG, ZHENSHEN YANG, LINGYING YE, and JIANGUO TANG

The effects of Mn or Zr additions on the dispersoid formation and recrystallization behavior in Al-Zn-Mg alloys were investigated. The combined additions of Mn and Zr are expected to increase the uniformity of dispersoids and increase the sizes of Al_3Zr and Al_6Mn dispersoids but decrease their volume fraction, which reduces the pinning force of dispersoids to grain boundaries. Al_6Mn dispersoids are incoherent with the Al matrix and result in lower pinning force compared to that of Al_3Zr dispersoids. Consequently, the inhibiting effect of combined additions of Mn and Zr on recrystallization is not as strong as that due to Zr addition alone. After hot rolling, the long axis of most ellipsoidal Al_6Mn dispersoids tends to be parallel to the rolling direction (RD), resulting in a larger pinning force in the normal direction (ND) than in the RD; therefore, the aspect ratios of recrystallized grains are larger in Mn-containing alloys than in Mn-free alloys. Further, the addition of Mn in Al-Zn-Mg alloy can lead to coarse α-AlFeMnSi constituent particles and, therefore, a higher area fraction of second phase in Mn-containing alloys; as a result, particle-stimulated nucleation (PSN) is the dominant recrystallization mechanism in Mn-containing alloys, while both PSN and strain-induced grain boundary migration (SIBM) exist in Zr-containing alloys.

https://doi.org/10.1007/s11661-019-05368-w

I. INTRODUCTION

MICROALLOYING is an effective way to inhibit recrystallization and, therefore, improve properties of aluminum alloys.[1–6] The additions of transition elements or rare earth elements lead to the formation of various dispersoids, which can pin grain boundaries.[7–10] For instance, a small addition of Zr to Al-Zn-Mg alloys can lead to the formation of coherent $L1_2$ Al_3Zr dispersoids, which can offer a strong Zener-drag effect on grain boundaries during solution heat treatment.[11,12] However, Zr tends to segregate to dendrite/grain centers during casting (since the partition coefficient $K > 1$),[13] and the concentration gradients cannot be removed during subsequent heat treatment.[14] As a result, there is a higher number density of Al_3Zr dispersoids in the interior of the dendrite/grain than near the dendrite/grain boundaries, and a particle-free zone often exists adjacent to grain boundaries and leads to partial recrystallization in the deformed alloy after solution heat treatment.

The addition of Mn to aluminum may lead to various Mn-containing dispersoids, such as Al_3Mn, Al_4Mn, and Al_6Mn,[15,16] and in multicomponent alloys containing Zn, Mg, or Cu, dispersoids such as $Al_{20}Cu_2Mn_3$, $Al_{24}Mn_5Zn$, and $Al_{20}(Zn,Cu)_2Mn_3$ can form.[17–19] In 2XXX, 5XXX, and 6XXX series aluminum alloys, it has been reported that Mn-containing dispersoids play an important role in the control of recrystallization behavior and refining recrystallized grains.[20–24] Mn tends to segregate toward the dendrite/grain boundaries (partition coefficient < 1) during casting.[25] Therefore, the number density of Mn-containing dispersoids in dendrite/grain boundaries is higher than that in the interior of the dendrite/grain. Based on their opposite microsegregation patterns, the combined additions of Mn and Zr are expected to create a greater uniformity of dispersoid coverage and, consequently, increase recrystallization resistance.

SHENGDAN LIU, LINGYING YE, and JIANGUO TANG are with the School of Materials Science and Engineering, Central South University, Changsha 410083, China and with the Key Laboratory of Non-ferrous Metals Science and Engineering, Ministry of Education, Changsha 410083, China and also with the Nonferrous Metal Oriented Advanced Structural Materials and Manufacturing Cooperative Innovation Center, Changsha 410083, China. Contact email: lingyingye@csu.edu.cn JINGCHAO CHEN, WENRU CHAI, QING WANG, and ZHENSHEN YANG are with the School of Materials Science and Engineering, Central South University and also with the Key Laboratory of Non-ferrous Metals Science and Engineering.

Manuscript submitted December 13, 2018.
Article published online July 26, 2019

In fact, the combined additions of Mn and Zr exhibit different effects on recrystallization behavior in different aluminum alloys. For instance, Walsh *et al.*[26] found the addition of Mn from 0.31 to 1.02 wt pct had little effect on recrystallization of 2134-type Al alloys and all the alloys were in the unrecrystallized condition. Cheong and Weiland.[27] reported that the combined additions of Mn and Zr increase recrystallization resistance of Al-Cu-Mg alloys, but the mechanism was not discussed. In contrast, Tsivoulas *et al.*[28] showed that the combined additions of Mn and Zr are detrimental to recrystallization resistance in Al-Cu-Li alloys, because the presence of Mn increases the size and reduces the number density of Al_3Zr. In Al-Mg alloys, Kim *et al.*[23] found that the combined additions of Zr and Mn are detrimental to recrystallization resistance at temperatures below 452 °C but beneficial above 452 °C. This phenomenon is due to the different recrystallization mechanisms in different temperature ranges.

Al-Zn-Mg alloys are widely used in aerospace, transportation, and military fields due to their high strength and low density.[29–33] It is often desirable to inhibit recrystallization during solution heat treatment so as to improve the strength, fracture toughness, corrosion resistance, and quench sensitivity of these alloys.[34–39] Mn and Zr are often added to these alloys and have been found to inhibit recrystallization effectively. For instance, Yamada and Tanaka[40] found that the addition of Mn (0.2 to 0.7 wt pct) or Zr (0.1 to 0.2 wt pct) has a significant effect of retarding growth of recrystallized grains in Al-4.5 pct Zn-1.5 pct Mg alloys. Miyata and Yoshihara[41] found that the combined additions of Mn and Zr (0.18 wt pct Mn + 0.1 wt pct Zr, 0.3 wt pct Mn + 0.03 wt pct Zr) and single addition of Mn or Zr have the same effect on recrystallization suppression in Al-4.5 pct Zn-0.9 pct Mg alloys, but the mechanism was not clear. An attempt was made in this work to clarify this issue to achieve better understanding of the microalloying mechanism of Mn and Zr in Al-Zn-Mg alloys.

II. EXPERIMENT

Four Al-Zn-Mg alloy DC ingots were used in this work, and the chemical compositions calibrated by inductively coupled plasma–atomic emission spectroscopy are shown in Table I. The ingots were homogenized by heating slowly to 460 °C, holding for 24 hours in an air furnace, and then cooling in still air. After preheating at 450 °C for 1 hour, the ingots were hot rolled from 30- to 3-mm sheets by multipasses. Then, the sheets were heated to 470 °C in an air furnace for solution heat treatment, held for 1 hour, and finally cooled in room temperature water.

A ZEISS EVO/MA10 scanning electron microscope (SEM) with energy-dispersive X-ray spectroscopy (EDS) and an electron backscattered diffraction (EBSD) system was used to examine second phases and grain structure. The samples for SEM and EBSD examination were thinned carefully to foils with a thickness of about 0.1 mm, punched into small disks of 3 mm in diameter, and then electropolished in a solution containing 30 pct HNO_3 and 70 pct CH_3OH below − 20 °C in liquid nitrogen. EBSD data were analyzed by HKL Channel 5 software. Grain boundaries with misorientation angles between 2 and 15 deg were defined as low-angle grain boundaries (LAGBs), and those with misorientation angles beyond 15 deg were defined as high-angle grain boundaries (HAGBs).[2]

A JXA-8230 electron-probe microanalyzer (EPMA) was used to measure the element distribution across grain boundaries in the as-cast ingots, and a step size of 1 μm and a voltage of 20 kV were applied. The dispersoids in the ingots after homogenization were examined on a Tecnai G^2 F20 transmission electron microscope (TEM) with EDS operated at 200 kV. To examine the dispersoids in the rolled sheets after solution heat treatment, a Titan G^2 60-300 scanning transmission electron microscope (STEM) with a high-angle annular dark field (HAADF) detector operated at 300 kV was used. The samples for TEM and STEM studies were thinned to foils of 0.1 mm and punched into disks of 3 mm in diameter; then, they were electropolished in a solution containing 30 pct HNO_3 and 70 pct CH_3OH below − 20 °C in liquid nitrogen.

III. RESULTS

A. *Grain Structure and Coarse Second Phase*

After hot rolling, grains were elongated along the rolling direction (RD) and banded deformed structures with recovered subgrains can be seen. As an example, Figure 1(a) shows the EBSD map of as-rolled Al-Zn-Mg sheet. There are a number of subgrains with sizes from about 1 to 3 μm. It is known that the stored energy of subgrains in the deformed specimen plays a key role in static recrystallization. The stored energy U_{sg} can be estimated using the following relationship[42]:

$$U_{sg} \approx \frac{3\gamma_{\mathrm{HAB}}}{d}\frac{\theta}{\theta_m}\left(1 - \ln\frac{\theta}{\theta_m}\right) \quad [1]$$

where θ is the average boundary misorientation, γ_{HAB} is the energy of the HAGB, and the cutoff θ_m is taken as 15 deg.[43] Values of the average misorientations of the LAGBs (θ) and the equivalent subgrain circular diameter (d) were obtained from EBSD orientation maps. Figure 1(b) shows the estimated average stored energy in the four rolled sheets. Al-Zn-Mg-Mn sheet has the highest stored energy, followed by Al-Zn-Mg-Mn-Zr sheet and Al-Zn-Mg-Zr sheet, and Al-Zn-Mg sheet has the lowest stored energy. The addition of Mn can significantly increase stored energy of Al-Zn-Mg alloy sheets; however, the addition of Zr results in a slight increase in the stored energy. This may be because the addition of Mn or Zr results in different particles and the density of dislocations is proportional to the ratio of the volume fraction of the particles to the radius, resulting in different deformation stored energy.[44]

Figures 2 and 3 show typical EBSD maps and SEM images of the four sheets after solution heat treatment,

Table I. Chemical Compositions of Alloys Used in This Work (Weight Percent)

Alloys	Zn	Mg	Cu	Mn	Zr	Fe	Si	Al
Al-Zn-Mg	4.33	1.24	0.14	0.00	0.00	< 0.16	< 0.1	bal.
Al-Zn-Mg-Mn	4.29	1.23	0.15	0.29	0.00	< 0.16	< 0.1	bal.
Al-Zn-Mg-Zr	4.33	1.28	0.16	0.00	0.13	< 0.16	< 0.1	bal.
Al-Zn-Mg-Mn-Zr	4.31	1.19	0.15	0.28	0.12	< 0.16	< 0.1	bal.

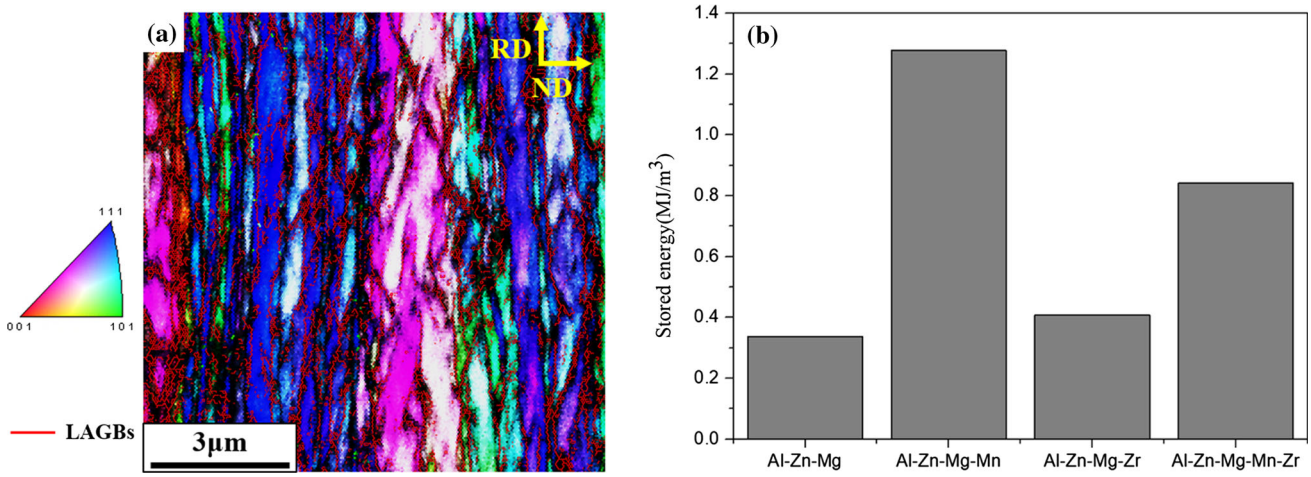

Fig. 1—(*a*) EBSD map of as-rolled Al-Zn-Mg sheet. (*b*) Calculated average stored energy in the rolled Al-Zn-Mg alloy sheets.

and the results of grain structure and second phase are summarized in Table II. It can be seen from Figures 2(a) and (c) that the addition of Mn has significant effects on the grain structure of Al-Zn-Mg sheet. After solution heat treatment, complete recrystallization occurs in Al-Zn-Mg sheet and quite large equiaxed grains can be seen. Complete recrystallization also occurs in Al-Zn-Mg-Mn sheet, but the grains are apparently smaller. The grain sizes along the RD and the normal direction (ND) were measured using the line intercept method, and the results are shown in Table II. The average sizes of recrystallized grains along both the RD and ND are larger in Al-Zn-Mg sheet than in Al-Zn-Mg-Mn sheet, indicating that the growth of recrystallized grains is significantly inhibited by Mn. This is similar to Yamada and Tanaka's findings[40] that the addition of Mn (0.2 to 0.7 wt pct) can retard grain growth in Al-4.5 pct Zn-1.5 pct Mg alloys.

As shown in Figures 3(a) and (e) and Table II, partial recrystallization occurs in both Al-Zn-Mg-Zr and Al-Zn-Mg-Mn-Zr sheets after solution heat treatment. The Zr addition alone exhibits the best recrystallization suppression effect with a recrystallization fraction of only about 34 pct; the average sizes of recrystallized grains are about 10.2 and 7.7 μm in the RD and ND, respectively. The combined additions of Mn and Zr lead to a large number of recrystallized grains (Figure 3(e)) with a higher recrystallization fraction of about 84 pct; the average sizes of recrystallized grains are 16.7 μm in the RD and 9.4 μm in the ND. Moreover, the shape of recrystallized grains changes after adding minor elements. In Al-Zn-Mg sheet, most grains exhibit an equiaxed shape and their aspect ratio is about 1.09. In Al-Zn-Mg-Mn and Al-Zn-Mg-Zr sheets, most recrystallized grains are elongated along the RD and their aspect ratios are about 1.45 and 1.33, respectively. After the combined additions of Mn and Zr, most recrystallized grains are further elongated along the RD with the aspect ratio increasing to be about 1.78.

It was also found that the number of recrystallized grains increases greatly with the additions of Mn and Zr (Table II), and this may be related to the difference in the recrystallization mechanism. To better understand these issues, coarse second-phase particles were examined by SEM and typical images are given in Figures 2(b), (d) and 3(b), (f). The orientation of grains is also indicated in Figures 2 and 3, and the volume fraction of different textures was calculated and is given in Table II. Compared with Al-Zn-Mg sheet, there are larger amounts of coarse particles with sizes greater than about 1 μm in Al-Zn-Mg-Mn sheet (Figures 2(b) and (d)) and their area fraction increases significantly from 0.13 to 0.62 pct. According to EDS analysis, coarse particles in Al-Zn-Mg sheet mainly contain (wt pct) Fe: 17.4 to 22.5, Si: 0.4 to 3.3, Zn: 2.1 to 3.5, Mg: 0.3 to 1.2, and Al: bal and they are likely Al_8Fe_2Si phase.[45] In Al-Zn-Mg-Mn sheet, besides this phase, some coarse particles were found to mainly contain (wt pct) Mn:

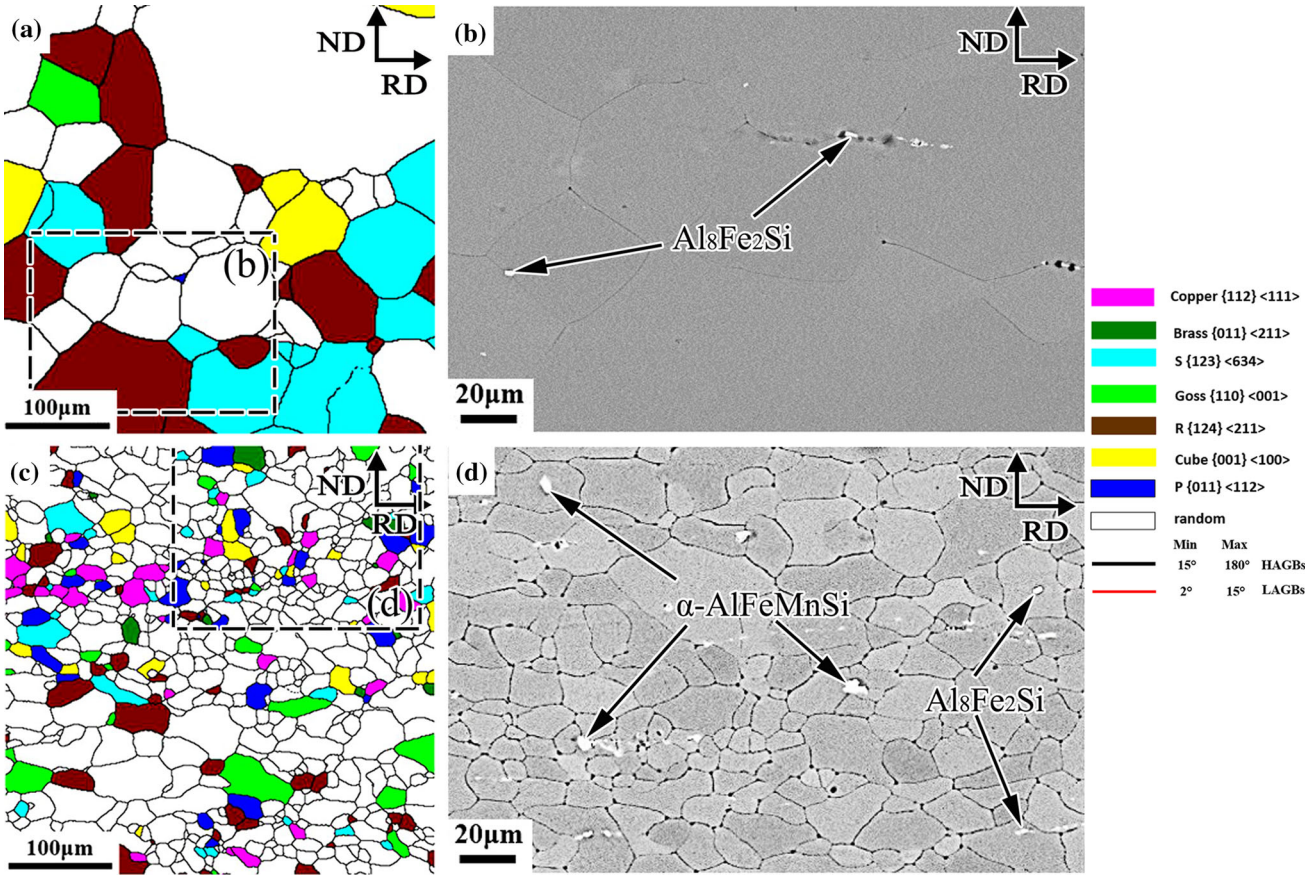

Fig. 2—EBSD texture component maps showing recrystallized grains with various orientations: (*a*) Al-Zn-Mg sheet and (*c*) Al-Zn-Mg-Mn sheet. SEM images showing second phases of the region in the dotted box in EBSD maps: (*b*) Al-Zn-Mg sheet and (*d*) Al-Zn-Mg-Mn sheet.

2.0 to 6.7, Fe: 18.6 to 25.7, Si: 1.6 to 4.2, Zn: 1.5 to 3.0, Mg: 0.2 to 0.7, and Al: bal. and they are likely α-AlFeMnSi phase.[46] It is known that coarse second-phase particles can favor recrystallization *via* the particle-stimulated nucleation (PSN) mechanism in many Al alloys.[47–51] During plastic deformation, it is often difficult for coarse particles to deform and the interface between these particles and the Al matrix hinders the movement of dislocations. As a result, there are severely deformed zones with high stored energy around the coarse particles, which leads to recrystallization nuclei during annealing or solution heat treatment. PSN is generally found to occur in particles with sizes larger than approximately 1 μm and lead to recrystallized grains with random orientations. As shown by the EBSD map in Figures 2(c) and (d), most recrystallized grains around coarse particles (> 1 μm) are randomly oriented. Further, the proportion of randomly oriented grains increased from 35.05 to 74.45 pct with the addition of Mn (Table II). These results indicate that PSN is the dominant recrystallization mechanism in Al-Zn-Mg-Mn sheet.

In Al-Zn-Mg-Zr sheet, coarse particles can be seen in some recrystallized grains with random orientation (Figures 3(a) and (b)), and it is likely that these grains formed *via* the PSN mechanism. In addition, strain-induced grain boundary migration (SIBM)[52–54] may occur during recrystallization in this sheet. The difference in the stored energy on opposite sides of the grain boundary is presumed to be the driving force for SIBM.[47] As shown in Figures 3(c) and (d), for instance, there are a number of small subgrains in the recovered regions, which have higher stored energy.[42,43] This is favorable for the occurrence of SIBM. In Figure 3(c), it is likely that the recrystallized grains with Brass orientation moved along the direction indicated by yellow arrows and grew into the neighboring recovered deformed band with Brass orientation; in Figure 3(d), the recrystallized grains with S orientation may form in a similar manner. In the heavily rolled aluminum alloys, Brass and S orientations are typical deformed texture.[55] SIBM involves the bulging of part of an original grain boundary; therefore, a characteristic feature is that the orientation of newly formed recrystallized grains is similar to that of the old grains from which they have grown. These results imply that SIBM occurred in this sheet during solution heat treatment.

In Al-Zn-Mg-Mn-Zr sheet, PSN is likely the dominant recrystallization mechanism because random texture is dominant (Table II). The number of coarse

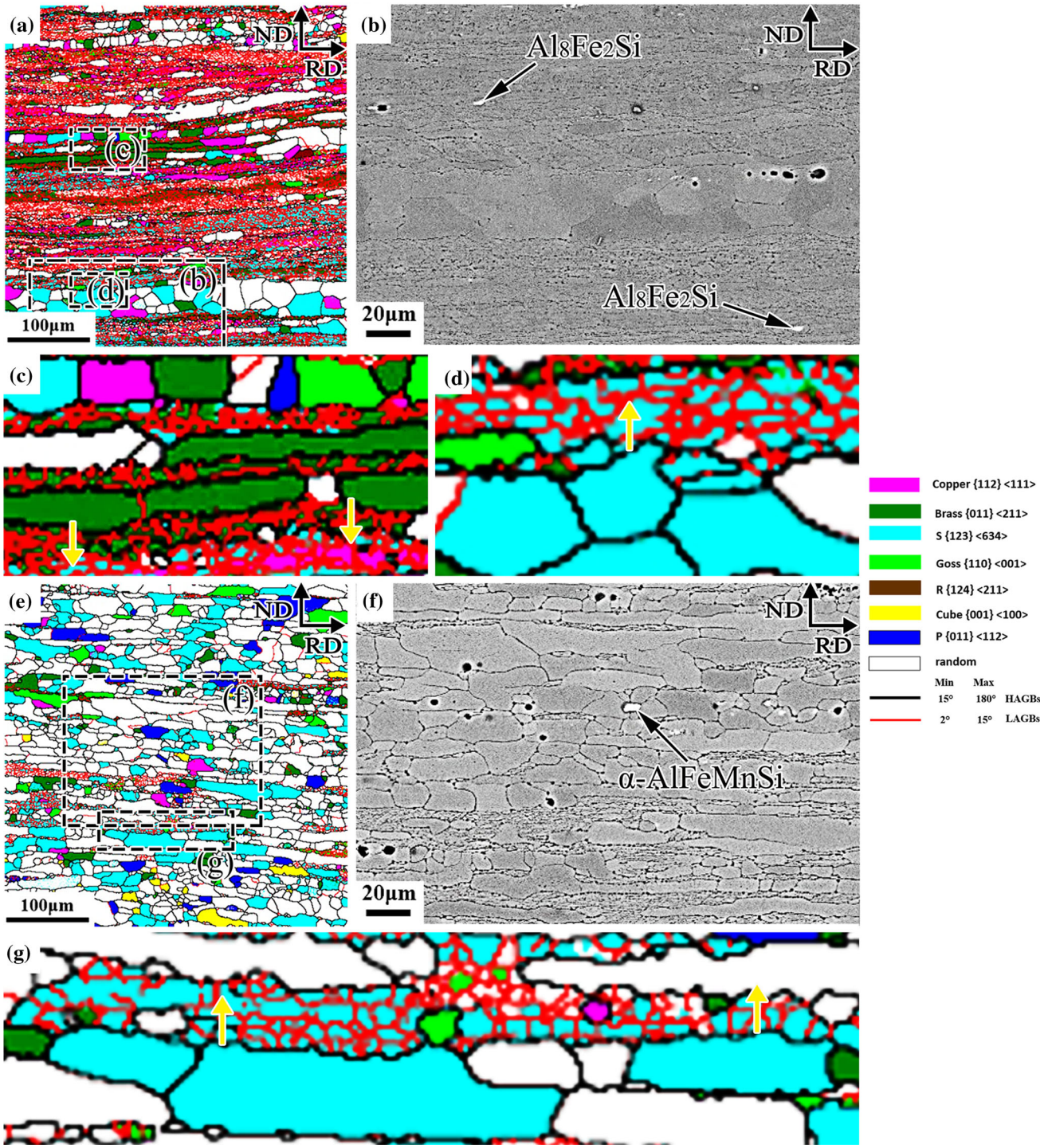

Fig. 3—EBSD texture component maps showing grains with various orientations: (*a*), (*c*), and (*d*) Al-Zn-Mg-Zr sheet and (*e*) and (*g*) Al-Zn-Mg-Mn-Zr sheet. SEM images showing second phases of the region in the dotted box in EBSD maps: (*b*) Al-Zn-Mg-Zr sheet and (*f*) Al-Zn-Mg-Mn-Zr sheet.

particles is high in this sheet, and most recrystallized grains with coarse particles are randomly oriented (Figures 3(e) and (f)). SIBM may play an important role, as the total fraction of Copper, Brass, and S texture is about 30 pct. For instance, as shown in Figure 3(g), some recrystallized grains with S orientation grew into the neighboring recovered deformed band with S orientation.

Table II. Results of Grain Structure, Texture, and Second Phase from EBSD and SEM Analyses

Alloys	Sizes of Recrystallized Grains in RD (μm)	Sizes of Recrystallized Grains in ND (μm)	Aspect Ratio (RD/ND)	Recrystallization Fraction (Pct)	Number of Recrystallized Grains (mm^2)	Area Fraction of Second Phases (Pct)	Fraction of Different Textures (Pct)							
							Copper	Brass	S	Goss	R	Cube	P	Random
Al-Zn-Mg	46.78 ± 4.59	42.71 ± 3.65	1.09 ± 0.06	100	365 ± 18	0.13	—	—	17.9	1.74	40.5	4.81	—	35.05
Al-Zn-Mg-Mn	19.46 ± 3.14	13.43 ± 2.96	1.45 ± 0.12	100	3667 ± 32	0.62	3.08	1.13	3.01	4.30	8.04	2.32	3.67	74.45
Al-Zn-Mg-Zr	10.19 ± 2.48	7.68 ± 2.37	1.33 ± 0.15	34	1800 ± 76	0.33	12.7	14.1	33.8	2.28	6.88	—	0.096	30.144
Al-Zn-Mg-Mn-Zr	16.73 ± 2.16	9.41 ± 2.85	1.78 ± 0.22	84	4640 ± 12	0.78	0.94	3.92	25.1	—	4.19	2.96	4.82	58.07

B. *Features of Dispersoids*

The primary purpose of the addition of Mn and Zr is to form dispersoids, which are expected to inhibit recrystallization. Attention has been paid to the features of dispersoids in different alloys.

1. *Dispersoids in the homogenized alloys*

Figure 4 gives TEM images showing dispersoids in the ingots after homogenization. It can be seen that there is a great quantity of dispersoids near the grain boundary in Al-Zn-Mg-Mn alloy, but their number tends to decrease with the increase of distance from the grain boundary to the interior of the grain (Figures 4(a) through (c)). Most dispersoids exhibit an ellipsoidal shape, and some exhibit a platelike shape. The $\langle 011 \rangle_{Al}$ selected area diffraction pattern (SADP) inset in Figure 4(b) indicates that these dispersoids are Al_6Mn phase[56] and they are incoherent with the Al matrix. In the Al-Zn-Mg-Zr alloy, as expected, the dispersoids in the matrix are Al_3Zr phase, as indicated by the $\langle 001 \rangle_{Al}$ SADP in Figure 4(e); moreover, most of them exhibit the characteristic coffee-bean contrast, indicating that they are coherent with the Al matrix. There are almost no Al_3Zr dispersoids near the grain boundary (Figure 4(d)), but their number tends to increase toward the grain center (Figures 4(e) and (f)). In the Al-Zn-Mg-Mn-Zr alloy, both Al_6Mn and Al_3Zr dispersoids can be found (Figures 4(g) through (i)) and their distribution is similar to that in the Al-Zn-Mg-Mn and Al-Zn-Mg-Zr alloys. This feature is due to the different segregation behaviors of Mn and Zr during casting. As an example, Figure 5 shows the concentration distribution of Mn and Zr elements in the Al-Zn-Mg-Mn-Zr alloy ingot. It is seen that Mn tends to segregate toward the grain boundary and Zr tends to segregate toward the grain center in the as-cast ingot, leading to the different precipitation behaviors of Al_6Mn and Al_3Zr dispersoids in Al-Zn-Mg-Mn-Zr alloy after homogenization. In addition, it can be seen that there are some coarse Mn-rich particles at the grain boundaries in the Mn-containing alloys (Figures 4(a) through (g)).

It was found that pre-precipitated $MgZn_2$ particles were favorable nucleation sites for Al_3Zr dispersoids in Al-Zn-Mg alloys.[57,58] Mn-containing dispersoids are known to precipitate earlier than Zr-containing dispersoids primarily because of the higher diffusion rate of Mn in the Al matrix.[59–61] Thus, heterogeneous nucleation of Al_3Zr on pre-existing Al_6Mn dispersoids may occur, and Al_3Zr dispersoids can sometimes be seen to be attached to Al_6Mn dispersoids (for example, the STEM-HAADF image shown in Figure 6(a)). However, when the TEM foil was tilted through a wide angle, the Al_3Zr particle was clearly seen to be separated from the Al_6Mn particle (Figure 6(b)). Therefore, heterogeneous nucleation of Al_3Zr on Al_6Mn is unlikely to have occurred during homogenization. Zr was found to be dissolved in Al_6Mn dispersoids. As an example (Figure 6(c)), there is about 0.57 wt pct Zr in the Al_6Mn particle. A number of Al_6Mn dispersoids in the Al-Zn-Mg-Mn alloy and Al-Zn-Mg-Mn-Zr alloy were examined, and their chemical compositions are given in

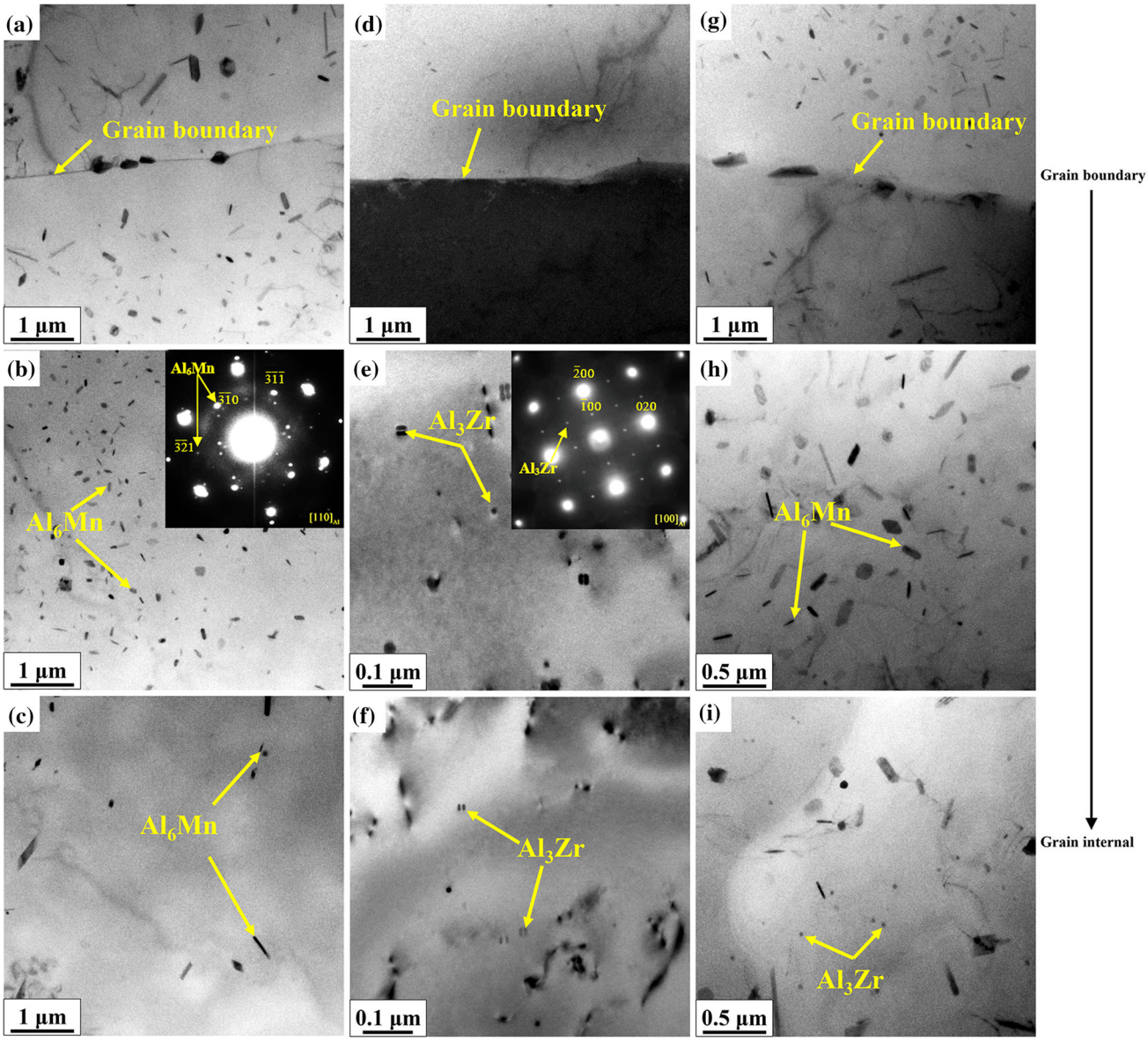

Fig. 4—Distribution of Mn- and Zr-containing dispersoids in homogenized alloys: (*a*) through (*c*) Al-Zn-Mg-Mn alloy, (*d*) through (*f*) Al-Zn-Mg-Zr alloy, and (*g*) through (*i*) Al-Zn-Mg-Mn-Zr alloy.

Table III. Al_6Mn dispersoids in the Al-Zn-Mg-Mn-Zr alloy contain about 0.38 wt pct Zr with concentration of other elements similar to those in the Al-Zn-Mg-Mn alloy. This phenomenon was also found in the Al-Mg alloy by Kaibyshev *et al.*, where small amounts of Zr can be dissolved in the Al_6Mn particles,[62] resulting in a lower concentration of Zr in the Al matrix.

2. *Dispersoids in rolled sheets after solution heat treatment*

Figure 7 shows STEM-HAADF images of Al_3Zr and Al_6Mn dispersoids in the sheets after solution heat treatment, and some parameters of these dispersoids were measured and are given in Table IV.

After rolling and solution heat treatment, recrystallized grains in Al-Zn-Mg-Mn sheet are covered by a number of Al_6Mn dispersoids (Figure 7(a)). These dispersoids did not inhibit recrystallization effectively, as complete recrystallization occurred in this sheet (Figure 2). Smaller recrystallized grains were obtained likely because Al_6Mn dispersoids retarded the migration of grain boundaries, and some Al_6Mn dispersoids are seen to be located at grain boundaries (Figures 7(a) and (b)). Most Al_6Mn dispersoids have an ellipsoidal shape, and their long axis tends to be parallel to the RD direction after rolling by comparing Figures 4(a) through (c) with Figures 7(a) and (b).

In Al-Zn-Mg-Zr sheet, recrystallized grains and unrecrystallized grains including subgrains, can be clearly distinguished. There are few Al_3Zr dispersoids in the recrystallized grains, while in the subgrain region, there is a high density of fine Al_3Zr dispersoids (Figures 7(c) and (d)). Combined with the results of Figures 4(d) through (f), it is believed that the nonuniform

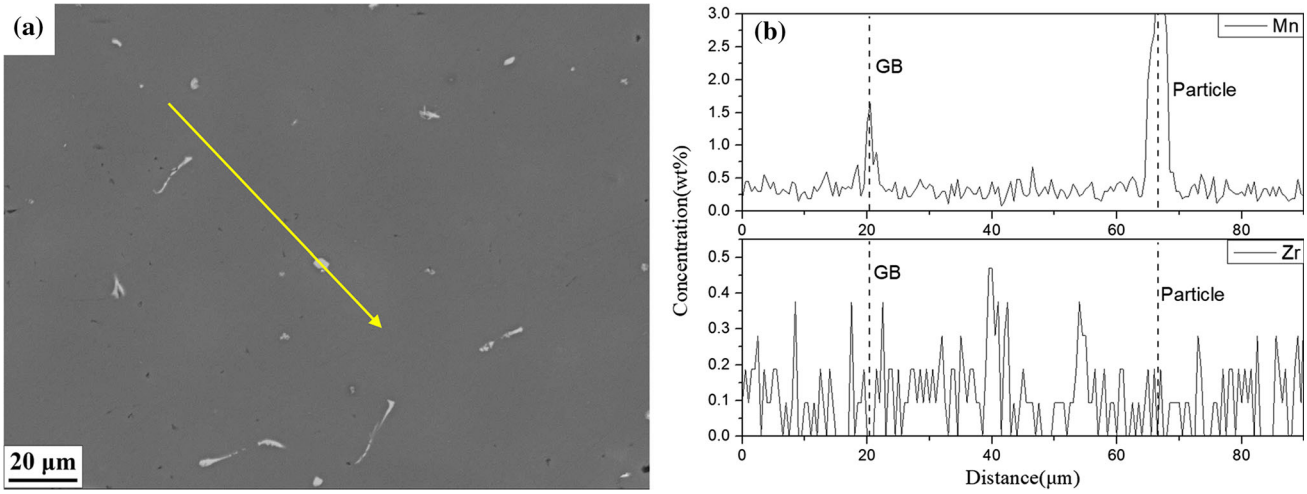

Fig. 5—(*a*) EPMA image showing the direction of line scanning in as-cast Al-Zn-Mg-Mn-Zr alloy. (*b*) The result of line scanning showing the Mn and Zr concentrations across grains.

distribution of Al_3Zr particles is the main reason for partial recrystallization of the Al-Zn-Mg-Zr alloy. This phenomenon has been discussed previously.[63] Based on Figures 2(c), 3(a), and 7(a), (c), it is reasonable to say the addition of Zr exhibits a better inhibition effect on recrystallization than Mn.

In Al-Zn-Mg-Mn-Zr sheet, Al_6Mn dispersoids are present in the recrystallized grains and in the subgrains (Figures 7(e) and (f)). Similarly, it can be observed that the long axis of the ellipsoidal Al_6Mn dispersoids tends to be parallel to the RD. Most Al_3Zr dispersoids are located in the subgrain region, which is similar to the case in Al-Zn-Mg-Zr sheet (Figures 7(c) and (d)). The average diameter of Al_3Zr dispersoids rises from 22.3 nm in Al-Zn-Mg-Zr sheet to 25.8 nm in Al-Zn-Mg-Mn-Zr sheet, with the number density and volume fraction decreasing from 82.7 to 41.7 μm^{-2} and 2.6×10^{-3} to 1.9×10^{-3}, respectively. This indicates that the addition of Mn leads to fewer and larger Al_3Zr dispersoids. In addition, the length and width of Al_6Mn dispersoids increase from 133.5 and 57.2 nm in Al-Zn-Mg-Mn sheet to 164.2 and 65.0 nm in Al-Zn-Mg-Mn-Zr sheet, respectively, and their number density reduces from 49.5 to 37.2 μm^{-2}. The combined additions of Mn and Zr lead to a more uniform coverage of dispersoids. Taking the effects of both Al_3Zr and Al_6Mn dispersoids into account, the f_v/r ratio is the maximum, 0.4 μm^{-1}, in the Al-Zn-Mg-Mn-Zr sheet (Table IV). However, the recrystallization resistance of Al-Zn-Mg-Mn-Zr sheet is not as high as expected and other factors must be taken in account.

IV. DISCUSSION

According to the results in Section III, Figure 8 shows the schematic of the main microstructural features in different alloys during processing and helps in better understanding the effect of combined additions of Mn and Zr on the formation of dispersoids and recrystallization behavior.

A. *Effect of Combined Additions of Mn and Zr on the Formation of Dispersoids*

During solidification of DC ingots, Mn and Zr tend to stay in the Al matrix to form a high supersaturated solid solution, which decomposes during subsequent homogenization. In the Al-Zn-Mg-Mn alloy, due to the segregation features of Mn (Figure 5), Al_6Mn dispersoids tend to precipitate near grain boundaries rather than in the interior of grains (Figure 8(a)). However, in the Al-Zn-Mg-Zr alloy, due to the segregation features of Zr (Figure 5), Al_3Zr dispersoids tend to precipitate in the interior of grains rather than near grain boundaries (Figure 8(d)). In the Al-Zn-Mg-Mn-Zr alloy, most Al_6Mn dispersoids are present near grain boundaries and most Al_3Zr dispersoids stay in the interior of grains (Figure 8(g)). The combined additions of Mn and Zr have a minor effect on the distribution of Al_6Mn and Al_3Zr dispersoids but change their parameters (Table IV). Al_6Mn dispersoids exhibit larger sizes, a lower number density, and lower volume fraction in the Al-Zn-Mg-Mn-Zr alloy compared with the Al-Zn-Mg-Mn alloy. Due to the coexistence of Mn and Zr, there is a higher concentration of total solute atoms in the solid solution, which can promote nucleation and rapid growth of Al_6Mn dispersoids. Consequently, Al_6Mn dispersoids with features in Figure 8(g) were obtained. Meanwhile, a small amount of Zr is incorporated within the Al_6Mn dispersoids (Table III), leading to a decreased supersaturation of Zr in the matrix. It is known that a decreased level of Zr results in a lower nucleation rate of Al_3Zr dispersoids and, hence, a lower particle number density.[60] As a result, Al_3Zr dispersoids exhibit larger sizes, lower volume fraction, and

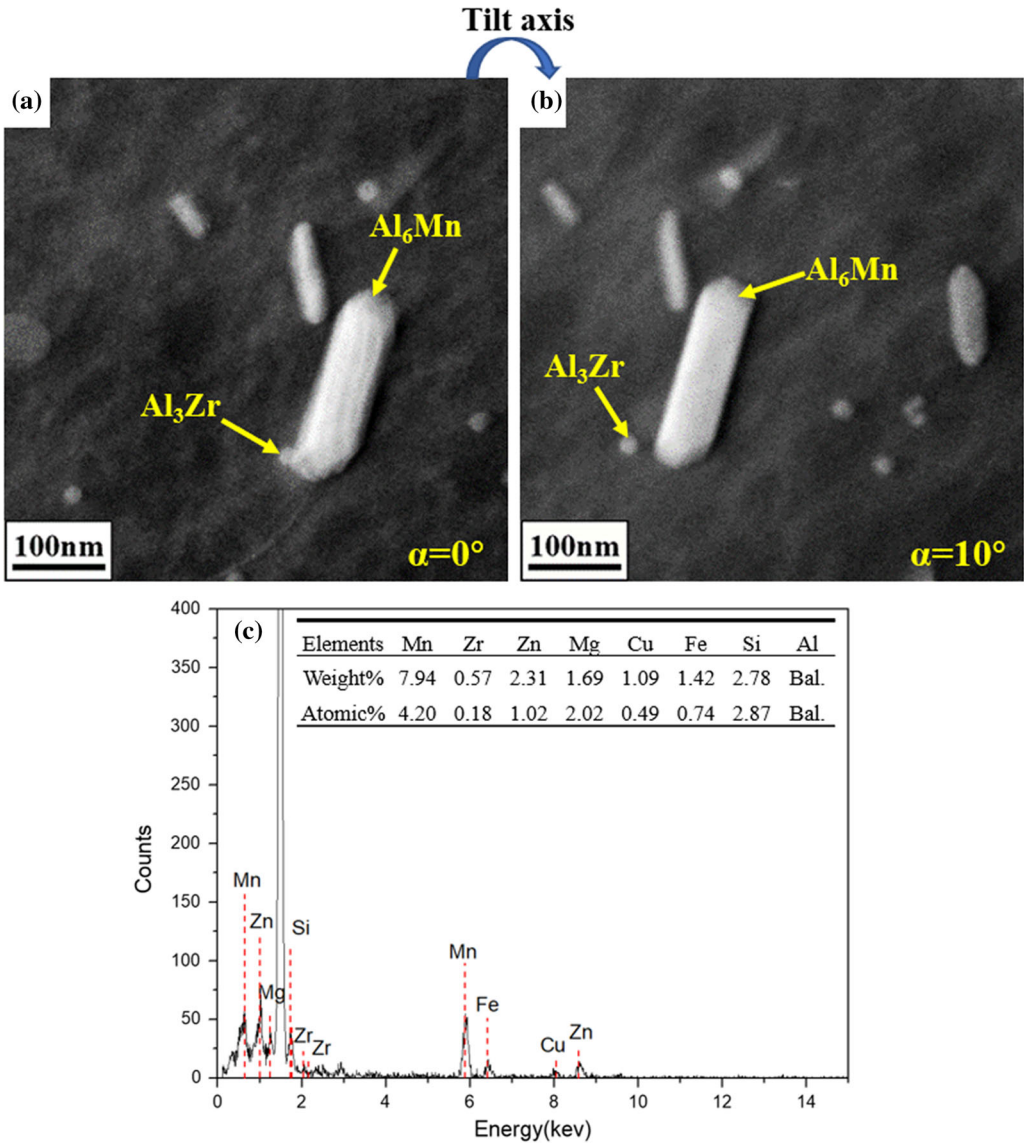

Fig. 6—(*a*) and (*b*) STEM-HAADF images from an example high-tilt series showing the physical interaction between Al_3Zr and Al_6Mn. (*c*) EDS result showing the chemical compositions of Al_6Mn phase.

Table III. Average Chemical Compositions of Al_6Mn Dispersoids in Al-Zn-Mg-Mn and Al-Zn-Mg-Mn-Zr Alloys (Weight Percent)

Alloys	Mn	Zr	Zn	Mg	Cu	Fe	Si	Al
Al-Zn-Mg-Mn	5.74 ± 1.10	—	4.66 ± 0.83	1.60 ± 0.15	0.90 ± 0.28	1.32 ± 0.40	1.17 ± 0.42	bal.
Al-Zn-Mg-Mn-Zr	5.64 ± 1.40	0.38 ± 0.09	5.11 ± 0.78	1.54 ± 0.18	0.90 ± 0.30	1.28 ± 0.80	1.03 ± 0.29	bal.

lower number density in the Al-Zn-Mg-Mn-Zr alloy compared with the Al-Zn-Mg-Zr alloy, and Al_3Zr dispersoids with the features in Figure 8(g) are obtained.

After rolling, both Al_6Mn and Al_3Zr dispersoids tend to distribute along the RD and exhibit a bandlike distribution (Figures 8(b), (e), and (h)). This phenomenon was observed in previous investigations.[38,64,65] The features of dispersoids have a significant effect on recrystallization behavior during subsequent solution heat treatment (Figures 8(c), (f), and (i)) and will be discussed in Section IV–B.

B. *Effect of Mn and Zr Additions on the Recrystallization Behavior*

It is well known that recrystallization is divided into two stages: the nucleation stage corresponding to the appearance of new grains and the growth stage during

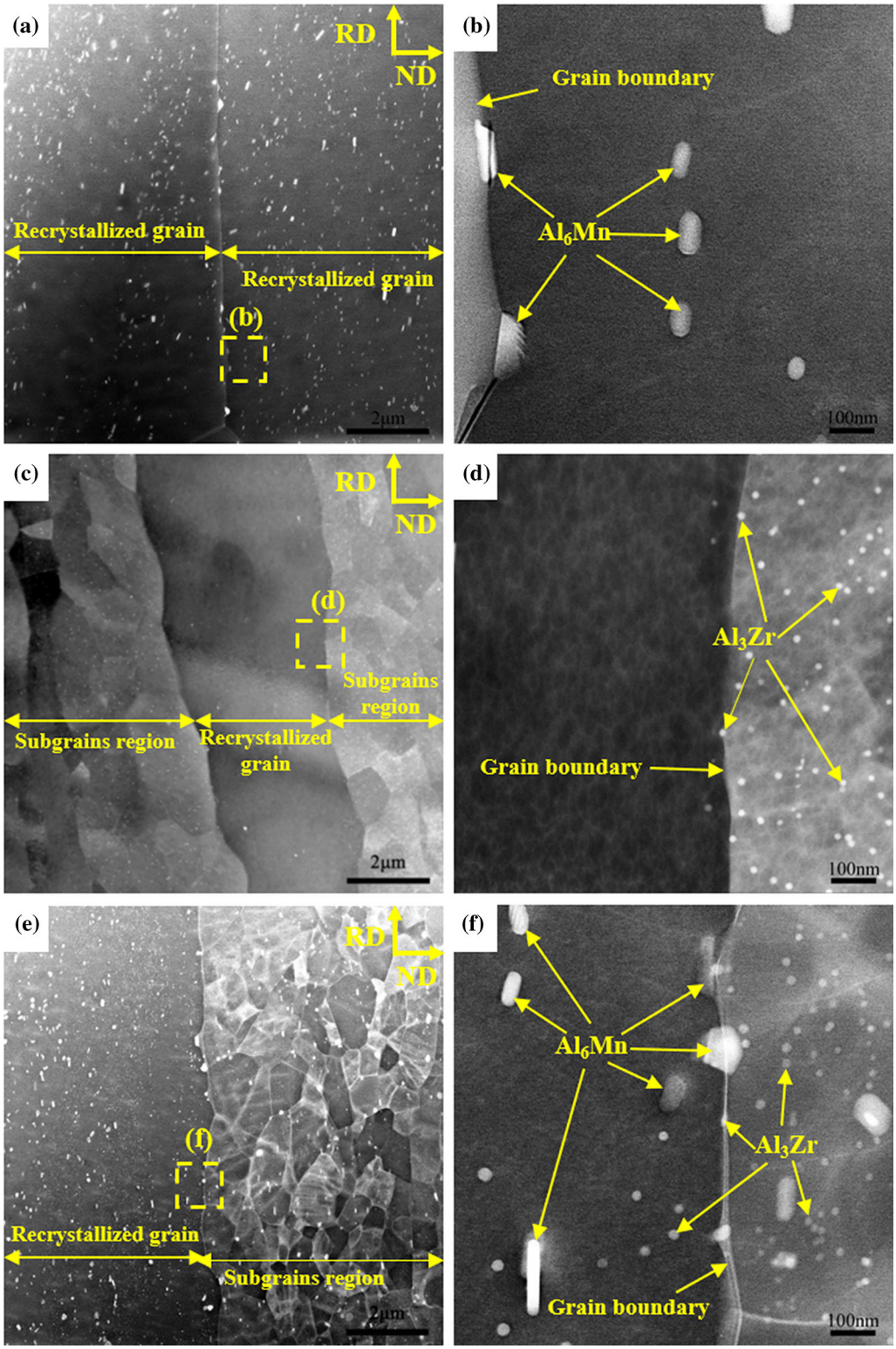

Fig. 7—STEM-HAADF images showing Al_3Zr and Al_6Mn dispersoids in the rolled sheets after solution heat treatment: (*a*) and (*b*) Al-Zn-Mg-Mn sheet, (*c*) and (*d*) Al-Zn-Mg-Zr sheet, and (*e*) and (*f*) Al-Zn-Mg-Mn-Zr sheet. (b), (d) and (f) Magnified images of the region in the dotted box in (a), (c), and (e), respectively.

which the new grains replace deformed regions.[47] As shown in Figure 1(b), the additions of Mn or Zr increase the stored energy in Al-Zn-Mg alloys after deformation; therefore, there is a high driving force for recrystallization. The number of grains per unit area may be used to compare the rate of nucleation for simplification.[47] After solution heat treatment, the numbers of recrystallized grains are about 365 mm^{-2}

Table IV. Some Parameters for the Dispersoids in Each Rolled Alloy Based on STEM Examination

Alloys	Size (nm)				Volume Fraction (10^{-3})		Number Density (μm^{-2})		Interparticle Spacing (nm)			f_v/r (μm^{-1})	
	Al_6Mn (Length)	Al_6Mn (Width)	Al_6Mn (Equivalent Circular Diameter)	Al_3Zr (Diameter)	Al_6Mn	Al_3Zr	Al_6Mn	Al_3Zr	Al_6Mn	Al_3Zr	Al_6Mn	Al_6Mn	Al_3Zr
Al-Zn-Mg-Mn	133.5 ± 14.1	57.2 ± 4.5	87.4		16.3 ± 1.4		49.5 ± 6.2		328.5		0.37		
Al-Zn-Mg-Zr				22.3 ± 2.3		2.6 ± 0.3		82.7 ± 10		66.4			0.23
Al-Zn-Mg-Mn-Zr	164.2 ± 15.5	65.0 ± 6.3	103.3	25.8 ± 1.7	13.1 ± 1.1	1.9 ± 0.4	37.2 ± 5.3	41.7 ± 8.4	344.1	85.2	0.25		0.15

in Al-Zn-Mg sheet, 3667 mm^{-2} in Al-Zn-Mg-Mn sheet, 1800 mm^{-2} in Al-Zn-Mg-Zr sheet, and 4640 mm^{-2} in Al-Zn-Mg-Mn-Zr sheet (Table II). This shows that the addition of Mn can obviously increase the number of nuclei. According to Figures 2 and 3 and Table II, it is because Mn can combine with Fe and Si to form a larger number of coarse particles, which leads to the PSN of recrystallization. This is reasonable because there is a higher fraction of random texture (Table II), which often results from the PSN of recrystallization.[66]

During the growth of newly formed grains, grain boundaries migrate and interact with dispersoids. The features of dispersoids play a key role in the recrystallization fraction and aspect ratios of recrystallized grains. The Zener pinning force (P_z) of the dispersoids can be expressed by the following equation[67,68]:

$$P_z = k\gamma\left(\frac{f_v}{r}\right) \quad [2]$$

where P_z is the Zener pinning force, k is a numerical constant dependent on geometry, f_v is the volume fraction of the dispersed particles, γ is the grain boundary energy, and r is the particle radius. The values of f_v/r were determined for Al_3Zr and Al_6Mn dispersoids in different sheets and are given in Table IV. In general, a higher f_v/r value means a higher pinning force on grain boundaries and, hence, a higher capability to arrest recrystallization.[44]

As shown in Table IV, the f_v/r ratio of dispersoids is the highest in Al-Zn-Mg-Mn-Zr sheet, intermediate in Al-Zn-Mg-Mn sheet, and lowest in Al-Zn-Mg-Zr sheet. Al-Zn-Mg-Mn-Zr sheet is, therefore, expected to have the best resistance to recrystallization; however, this sheet has a higher recrystallization fraction than Al-Zn-Mg-Zr sheet (Figure 3 and Table II). Thus, apart from the f_v/r value, the features of dispersoids, such as coherency and morphology, must be considered.[69] According to the summary of Huang *et al.*,[69,70] Figure 9 is used to show schematically the effect of particle coherency on the pinning force.

When a single particle B interacts with a moving flat boundary between grains A and C, the boundary meets the particle at D and E and there are three surface tensions, *i.e.*, the boundary tension, γ_{AC}, and two particle surface tensions, γ_{AB} and γ_{BC}. According to Smith,[67] for an incoherent particle, $\gamma_{AB} = \gamma_{BC}$ and $\beta = 90$ deg. The pinning force of particles on grain boundaries can be described as

$$F = 2\pi r \cos\alpha \cdot \gamma_{AC} \cdot \sin\alpha \quad [3]$$

The maximum pinning force is found to occur when $\alpha = 45$ deg:

$$F_{max} = \pi r \gamma_{AC} \quad [4]$$

There is a higher interface energy (γ_{BC}) when the grain boundary moves past a coherent particle, $\beta \neq 90$ deg, and the equilibrium of surface tensions and pinning force gives[69]

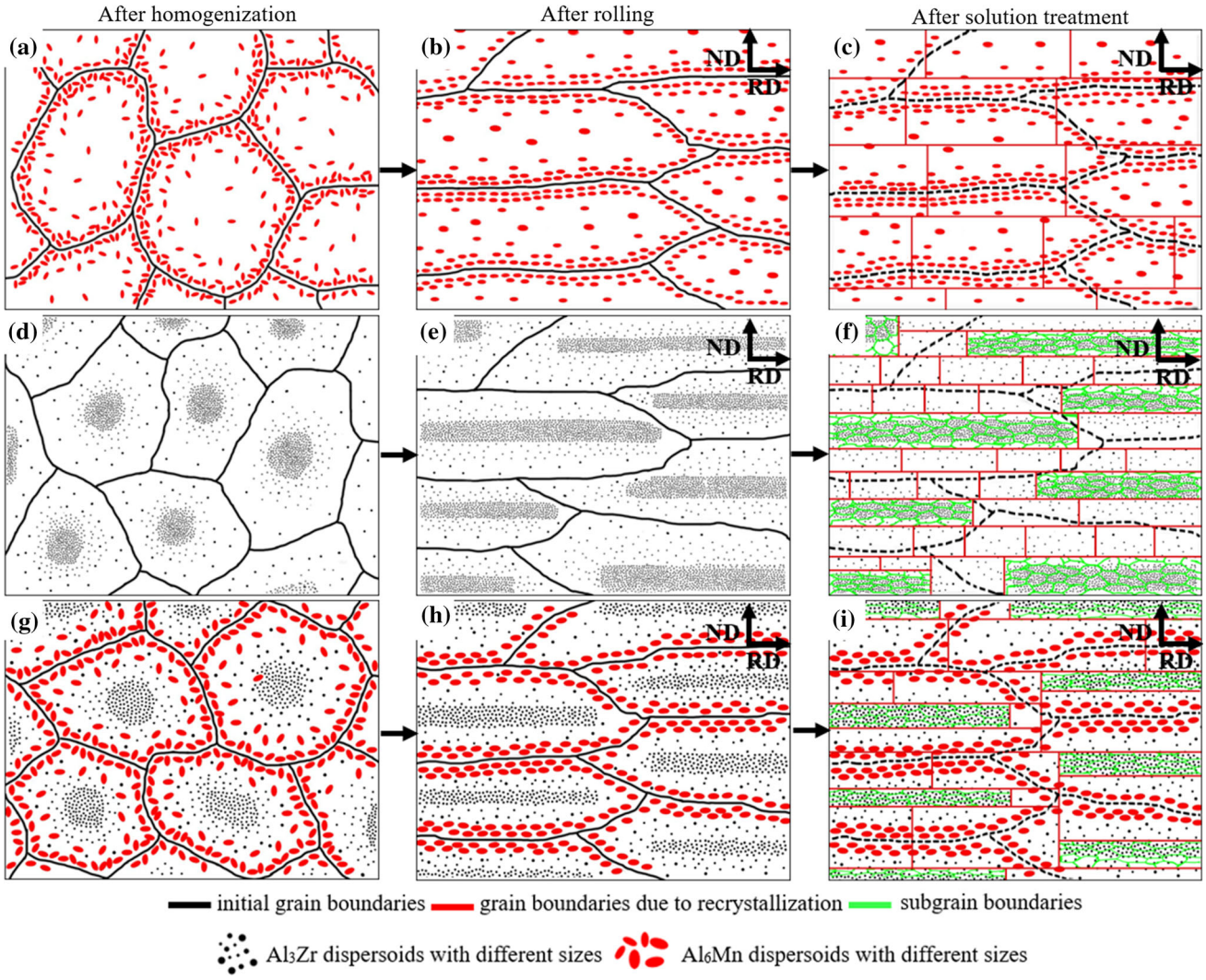

Fig. 8—Schematic of main microstructural features in different alloys during processing: (*a*) through (*c*) Al-Zn-Mg-Mn alloy, (*d*) through (*f*) Al-Zn-Mg-Zr alloy, and (*g*) through (*i*) Al-Zn-Mg-Mn-Zr alloy.

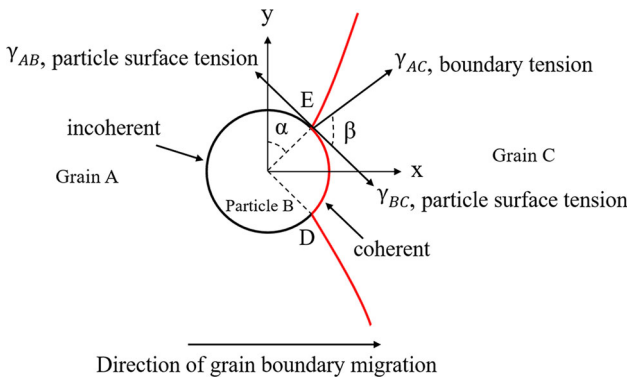

Fig. 9—Schematic graph showing the effect of particle coherency on pinning force.

$$\gamma_{BC} + \gamma_{AC} \cdot \cos\beta = \gamma_{AB} \quad [5]$$

$$F = 2\pi r \cos\alpha \cdot \gamma_{AC} \cdot \cos(180^\circ - \alpha - \beta) \quad [6]$$

The maximum pinning force is found to occur when $\alpha = 0$ deg and $\beta = 180$ deg:

$$F_{max} = 2\pi r \gamma_{AC} \quad [7]$$

As shown in Eqs. [3] through [7], the maximum pinning force from a coherent particle is twice that from an incoherent one of the same size. This means that the pinning force of coherent Al_3Zr dispersoids is significantly higher than that of incoherent Al_6Mn dispersoids. Moreover, Al_3Zr dispersoids exhibit a higher density and smaller sizes than Al_6Mn dispersoids. As a result, complete recrystallization occurred in Al-Zn-Mg-Mn sheet, but partial recrystallization occurred in Al-Zn-Mg-Zr sheet. In Al-Zn-Mg-Mn-Zr sheet, Al_3Zr dispersoids exhibit larger sizes, lower volume fraction, and lower number density (Table IV); therefore, they exert a lower pinning force on grain boundary migration compared with those in Al-Zn-Mg-Zr sheet. This contributes to the higher recrystallization fraction in

Al-Zn-Mg-Mn-Zr sheet than in Al-Zn-Mg-Zr sheet (Table II).

Moreover, the surface area of the particles that interact with the grain boundary is determined by the particle orientation.[69] Nes *et al.*[71] proposed that the pinning force of ellipsoidal particles in different directions can be calculated by

$$\text{Case I}: F_p^e = F_p^s \frac{2}{(1+\varepsilon)\varepsilon^{1/3}} \quad [8]$$

$$\text{Case II}: F_p^e = F_p^s \frac{1+2.14\varepsilon}{\pi\sqrt{\varepsilon}} \quad [9]$$

where F_p^e is the pinning force of an ellipsoidal particle, F_p^s is the pinning force of a spherical particle, and ε is the eccentricity of an ellipsoidal particle. Equations [8] and [9] apply when the long axis of the particle is perpendicular and parallel to the grain boundary, respectively. In Al-Zn-Mg-Zr sheet, Al_3Zr dispersoids are spherical; therefore, the pinning force in the RD is the same as that in the ND. However, due to the distribution features of Al_3Zr dispersoids shown in Figure 8(e), grain boundaries meet a higher density of particles when migrating along the ND than along the RD. As a result, for most recrystallized grains, the size is larger in the RD than in the ND (Figure 8(f)). In Mn-containing sheets, most Al_6Mn dispersoids are ellipsoidal and their long axis tends to be parallel to the RD (Figures 8(b) and (h)). Based on the data in Table IV, the pinning force of Al_6Mn dispersoids in the ND is about 2.80 and 3.10 times that in the RD, respectively, in Al-Zn-Mg-Mn sheet and Al-Zn-Mg-Mn-Zr sheet, indicating that these dispersoids exert a stronger dragging effect on grain boundary migration in the ND. Consequently, recrystallized grains tend to be elongated along the RD (Figures 8(c) and (f) and Table II). In Al-Zn-Mg-Mn-Zr sheet, recrystallized grains with larger aspect ratios are obtained due to the combined effect of Al_3Zr and Al_6Mn dispersoids.

V. CONCLUSIONS

1. The single addition of Mn refines recrystallized grains of Al-Zn-Mg sheet, though complete recrystallization occurs. The single addition of Zr leads to the lowest fraction of recrystallization and the minimum recrystallized grains. The combined additions of Mn and Zr result in partial recrystallization with the sizes of recrystallized grains and fraction of recrystallization larger than those in Al-Zn-Mg-Zr sheet.
2. The addition of Mn leads to coarse α-AlFeMnSi constituent particles and, therefore, a higher area fraction of coarse second-phase particles, which results in PSN. Consequently, random texture is dominant in Al-Zn-Mg-Mn sheet and Al-Zn-Mg-Mn-Zr sheet after solution heat treatment, and the number of recrystallized grains is larger in Mn-containing sheet than in Mn-free sheets. PSN is the dominant recrystallization mechanism in Mn-containing sheet. Both PSN and SIBM occur in Al-Zn-Mg-Zr sheet.
3. The addition of Zr exhibits higher capability than Mn to arrest recrystallization, because fine and coherent Al_3Zr dispersoids have higher pinning force on grain boundaries than incoherent Al_6Mn dispersoids. The combined additions of Mn and Zr have a minor effect on the distribution of Al_3Zr and Al_6Mn dispersoids but increase their sizes and decrease their volume fractions, leading to lower pinning force acting on grain boundaries.
4. The long axis of most ellipsoidal Al_6Mn dispersoids tends to be parallel to the RD after rolling and then the pinning force provided by Al_6Mn dispersoids is higher in the ND than in the RD, resulting in the larger size in the RD than the ND of the recrystallized grains in Mn-containing sheets. Due to the combined effect of Al_3Zr and Al_6Mn dispersoids, recrystallized grains in Al-Zn-Mg-Mn-Zr sheet exhibit the largest aspect ratio.

ACKNOWLEDGMENTS

This work is supported by the National Key Research and Development Program of China (Grant No. 2016YFB0300901), the Key Project of Science and Technology of Hunan Province (Grant No. 2016GK1004), and the Shenghua Yuying Project of Central South University (Grant No. 20130603).

REFERENCES

1. S.D. Liu, X.M. Zhang, M.A. Chen, J.H. You, and X.Y. Zhang: *Trans. Nonferrous Met. Soc.*, 2007, vol. 17, pp. 787–92.
2. Y. Deng, Z.M. Yin, K. Zhao, J.Q. Duan, and Z.B. He: *J. Alloys Compd.*, 2012, vol. 530, pp. 71–80.
3. N.H. Lee, P.W. Kao, T.Y. Tseng, and J.R. Su: *Mater. Sci. Eng. A*, 2012, vol. 535, pp. 297–305.
4. S.H.S. Ebrahimi, M. Emamy, N. Pourkia, and H.R. Lashgari: *Mater. Des.*, 2010, vol. 31, pp. 4450–56.
5. J.T.B. Gundersen, A. Aytaç, S. Ono, J.H. Nordlien, and K. Nişancıoğlu: *Corros. Sci.*, 2004, vol. 46, pp. 265–83.
6. Y.L. Wu, C. Li, F.H. Froes, and A. Alvarez: *Metall. Mater. Trans. A*, 1999, vol. 30A, pp. 1017–24.
7. Y.D. He, X.M. Zhang, and J.H. You: *Trans. Nonferr. Met. Soc.*, 2006, vol. 16, pp. 1228–35.
8. S.P. Wen, W. Wang, W.H. Zhao, X.L. Wu, K.Y. Gao, H. Huang, and Z.R. Nie: *J. Alloys Compd.*, 2016, vol. 687, pp. 143–51.
9. Y.B. Wang, Y. Lin, and J.M. Zeng: *Adv. Mater. Res.*, 2010, vols. 146–147, pp. 1874–77.
10. K.H. Chen, H.C. Fang, Z. Zhang, X. Chen, and G. Liu: *Mater. Sci. Eng. A*, 2008, vol. 497, pp. 426–31.
11. Y. Deng, Z.M. Yin, J.Q. Duan, K. Zhao, B. Tang, and Z.B. He: *J. Alloys Compd.*, 2012, vol. 517, pp. 118–26.
12. J.D. Robson and P.B. Prangnell: *Acta Mater.*, 2001, vol. 49, pp. 599–613.
13. K.P. Mingard, B. Cantor, I.G. Palmer, I.R. Hughes, P.W. Alexander, T.C. Willis, and J. White: *Acta Mater.*, 2000, vol. 48, pp. 2435–49.
14. Z.H. Jia, G.Q. Hu, B. Forbord, and J.K. Solberg: *Mater. Sci. Eng. A*, 2007, vol. 444, pp. 284–90.
15. Y.J. Li, W.Z. Zhang, and K. Marthinsen: *Acta Mater.*, 2012, vol. 60, pp. 5963–74.

16. B.O. Kong and S.W. Nam: *Mater. Lett.*, 1996, vol. 28, pp. 385–91.
17. E. Anselmino, A. Miroux, and S.V.D. Zwaag: *Mater. Charact.*, 2004, vol. 52, pp. 289–300.
18. K. Osamura, K. Kohno, H. Okuda, S. Ochiai, J. Kusui, K. Fujii, K. Yokoe, T. Yokota, and K. Hono: *Mater. Sci. Forum*, 1996, vols. 217–222, pp. 1829–34.
19. S.P. Dong and S.W. Nam: *Mater. Lett.*, 1994, vol. 13, pp. 716–18.
20. P. Ratchev and P. Jessner: *Mater. Sci. Forum*, 2014, vols. 794–796, pp. 1227–32.
21. I. Nikulin, A. Kipelova, S. Malopheyev, and R. Kaibyshev: *Acta Mater.*, 2012, vol. 60, pp. 487–97.
22. R. Hu, T. Ogura, H. Tezuka, T. Sato, and Q. Liu: *J. Mater. Sci. Technol.*, 2010, vol. 26, pp. 237–43.
23. Y.B. Kim, Y.H. Chung, K.K. Cho, and M.C. Shin: *Scripta Mater.*, 1997, vol. 36, pp. 111–16.
24. K. Kannan, J.S. Vetrano, and C.H. Hamilton: *Metall. Mater. Trans. A*, 1996, vol. 27A, pp. 2947–57.
25. R. Nadella, D.G. Eskin, Q. Du, and L. Katgerman: *Progr. Mater. Sci.*, 2008, vol. 53, pp. 421–80.
26. J.A. Walsh, K.V. Jata, and E.A. Starke: *Acta Metall.*, 1989, vol. 37, pp. 2861–71.
27. S.W. Cheong and H. Weiland: *Mater. Sci. Forum*, 2007, vols. 558–559, pp. 153–58.
28. D. Tsivoulas, J.D. Robson, C. Sigli, and P.B. Prangnell: *Acta Mater.*, 2012, vol. 60, pp. 5245–59.
29. C. Qin, G.Q. Gou, X.L. Che, H. Chen, J. Chen, P. Li, and W. Gao: *Mater. Des.*, 2016, vol. 91, pp. 278–85.
30. G. Gou, M. Zhang, H. Chen, J. Chen, P. Li, and Y.P. Yang: *Mater. Des.*, 2015, vol. 85, pp. 309–17.
31. T. Dursun and C. Soutis: *Mater. Des.*, 2014, vol. 56, pp. 862–71.
32. J.C. Williams and E.A. Starke, Jr: *Acta Mater.*, 2003, vol. 51, pp. 5775–99.
33. A. Heinz, A. Haszler, C. Keidel, S. Moldenhauer, R. Benedictus, and W.S. Miller: *Mater. Sci. Eng. A*, 2000, vol. 280, pp. 102–07.
34. H.C. Fang, H. Chao, and K.H. Chen: *J. Alloys Compd.*, 2015, vol. 622, pp. 166–73.
35. C. Krishnan, A.K. Kobylecky, and J.R. Kish: *Can. Metall. Q.*, 2015, vol. 54, pp. 349–58.
36. B. Li, Q.L. Pan, X. Huang, and Z. Yin: *Mater. Sci. Eng. A*, 2014, vol. 616, pp. 219–28.
37. N.M. Han, X.M. Zhang, S.D. Liu, D.G. He, and R. Zhang: *J. Alloys Compd.*, 2011, vol. 509, pp. 4138–45.
38. S.D. Liu, W.J. Liu, Y. Zhang, X.M. Zhang, and Y.L. Deng: *J. Alloys Compd.*, 2010, vol. 507, pp. 53–61.
39. F.S. Lin and E.A. Starke, Jr: *Mater. Sci. Eng.*, 1979, vol. 39, pp. 27–41.
40. H. Yamada and T. Tanaka: *J. Jpn. Inst. Light Met.*, 1989, vol. 39, pp. 32–37.
41. Y. Miyata and S. Yoshihara: *6th Int. Conf. on Aluminum Alloys*, 2012, pp. 1897–1902.
42. A. Godfrey, W.C. Cao, Q. Liu, and N. Hansen: *Metall. Mater. Trans. A*, 2005, vol. 36A, pp. 2371–78.
43. A. Lens, C. Maurice, and J.H. Driver: *Mater. Sci. Forum*, 2004, vols. 467–470, pp. 771–76.
44. M.F. Ashby: *Philos. Mag.*, 1966, vol. 14, pp. 1157–78.
45. A.R. Eivani, H. Ahmed, J. Zhou, and J. Duszczyk: *Metall. Mater. Trans. A*, 2009, vol. 40A, pp. 717–28.
46. W.C. Yang, S.H. Ji, X.R. Zhou, I. Stone, G. Scamans, G.E. Thompson, and Z.Y. Fan: *Metall. Mater. Trans. A*, 2014, vol. 45A, pp. 3971–80.
47. F.J. Humphreys and M. Hatherly: *Recrystallization and Related Annealing Phenomena*, 2nd ed., Elsevier, Oxford, United Kingdom, 2004, pp. 250–306.
48. B. Bay and N. Hansen: *Metall. Trans. A*, 1979, vol. 10A, pp. 279–88.
49. F.J. Humphreys: *Acta Mater.*, 1977, vol. 25, pp. 1323–44.
50. O. Engler, P. Yang, and X.W. Kong: *Acta Mater.*, 1996, vol. 44, pp. 3349–69.
51. R.D. Doherty, D.A. Hughes, F.J. Humphreys, J.J. Jonas, D. Juul Jensen, M.E. Kassner, W.E. King, T.R. McNelley, H.J. McQueen, and A.D. Rollett: *Mater. Sci. Eng. A*, 1997, vol. 238, pp. 219–74.
52. Y.Y. Zhang and J.S. Zhang: *Mater. Lett.*, 2011, vol. 65, pp. 1856–58.
53. S. Raveendra, H. Paranjape, S. Mishra, H. Weiland, R.D. Doherty, and I. Samajdar: *Mater. Sci. Eng. A*, 2009, vol. 40, pp. 2220–30.
54. P. Bate and B. Hutchinson: *Scripta Mater.*, 1997, vol. 36, pp. 195–98.
55. J. Sidor, A. Miroux, R. Petrov, and L. Kestens: *Acta Mater.*, 2008, vol. 56, pp. 2495–2507.
56. B.O. Kong, J.I. Suk, and S.W. Nam: *J. Mater. Sci. Lett.*, 1996, vol. 15, pp. 763–66.
57. Y.L. Deng, Y.Y. Zhang, L. Wan, A.A. Zhu, and X.M. Zhang: *Metall. Mater. Trans. A*, 2013, vol. 44A, pp. 2470–77.
58. H.Q. Lin, L.Y. Ye, L. Sun, T. Xiao, S.D. Liu, Y.L. Deng, and X.M. Zhang: *Trans. Nonferrous Met. Soc.*, 2018, vol. 28, pp. 829–38.
59. M. Vlach, I. Stulíková, B. Smola, H. Císařová, T. Kekule, J. Malek, D. Tanprayoon, and V. Neubert: *Def. Diffus. Forum*, 2013, vols. 334–335, pp. 161–66.
60. J.D. Robson: *Mater. Sci. Eng. A*, 2002, vol. 338, pp. 219–29.
61. T. Ohashi, L. Dai, and N. Fukatsu: *Metall. Trans. A*, 1986, vol. 17A, pp. 799–806.
62. R. Kaibyshev, F. Musin, D.R. Lesuer, and T.G. Nieh: *Mater. Sci. Eng. A*, 2003, vol. 342, pp. 169–77.
63. J.D. Robson and P.B. Prangnell: *Mater. Sci. Technol.*, 2002, vol. 18, pp. 607–14.
64. A. Deschampls and Y. Brechet: *Mater. Sci. Eng. A*, 1998, vol. 251, pp. 200–07.
65. K. Huang, O. Engler, Y.J. Li, and K. Marthinsen: *Mater. Sci. Eng. A*, 2015, vol. 628, pp. 216–29.
66. O. Engler: *Scripta Mater.*, 1997, vol. 37, pp. 1675–83.
67. C.S. Smith: *Trans. Am. Inst. Min. Eng.*, 1948, vol. 175, pp. 15–51.
68. P.A. Manohar, M. Ferry, and T. Chandra: *ISIJ. Int.*, 1998, vol. 38, pp. 913–24.
69. K. Huang, K. Marthinsen, Q. Zhao, and R.E. Logé: *Progr. Mater. Sci.*, 2018, vol. 92, pp. 284–359.
70. K. Huang and R.E. Logé: *Reference Module in Materials Science and Materials Engineering*, Elsevier, Oxford, United Kingdom, 2016, pp. 1–8.
71. E. Nes, N. Ryum, and O. Hunderi: *Acta Metall.*, 1985, vol. 33, pp. 11–22.